Implicit Active Contours Driven by Local Binary Fitting Energy

Chunming Li [1], Chiu-Yen Kao [2], John C. Gore [1], and Zhaohua Ding [1]

[1] Institute of Imaging Science
Vanderbilt University
Nashville, TN 37232-2310, USA
{chunming.li,john.gore,zhaohua.ding}@vanderbilt.edu

[2] Department of Mathematics
The Ohio State University
Columbus, OH 43210-1174, USA
kao@math.ohio-state.edu

Abstract

Local image information is crucial for accurate segmentation of images with intensity inhomogeneity. However, image information in local region is not embedded in popular region-based active contour models, such as the piecewise constant models. In this paper, we propose a region-based active contour model that is able to utilize image information in local regions. The major contribution of this paper is the introduction of a local binary fitting energy with a kernel function, which enables the extraction of accurate local image information. Therefore, our model can be used to segment images with intensity inhomogeneity, which overcomes the limitation of piecewise constant models. Comparisons with other major region-based models, such as the piecewise smooth model, show the advantages of our method in terms of computational efficiency and accuracy. In addition, the proposed method has promising application to image denoising.

1. Introduction

Active contour models have been one of the most successful methods for image segmentation [1, 3–7, 12]. The existing active contour models can be categorized into two classes: *edge-based models* [1,4–6] and *region-based models* [2,9,10]. These two types of models both have their pros and cons, and the choice of them in applications depends on different characteristics of images.

Edge-based models utilize image gradient to stop the evolving contours on the object boundaries. Typical edge-based active contour models have an edge-based stopping term and a balloon force term to control the motion of the contour. The edge-based stopping term serves to stop the contour on the desired object boundary. The balloon force term is introduced to shrink or expand the active contour so that the initial contour can be placed far away from the desired object boundary. However, appropriate choice of balloon force is sometimes difficult. If the balloon force is not large enough, the evolving contour may not able to pass some narrow parts of the object. If the balloon force is too large, the active contour is likely to pass through weak object boundary.

Region-based active contour models have the following advantages over edge-based models. First, region-based models do not utilize the image gradient and therefore have better performance for the image with weak object boundaries. Second, they are significantly less sensitive to the location of initial contours. One of the most popular region-based active contour models is Chan-Vese model [2]. This model has been successful for images with two regions, each having a distinct mean of pixel intensity. In [11], Vese and Chan extended their earlier work in [2] by using a multiphase level set formulation, in which multiple regions can be represented by multiple level set functions. These models are called *piecewise constant (PC) models*, since they assume that an image consists of *statistically homogeneous regions*. However, the regions of interest in images are often not statistically homogeneous, and therefore the PC models are not applicable to those types of images.

To handle more general scenario, Vese and Chan [11] and Tsai *et al.* [10] proposed two similar region-based active contour models, aiming at minimization of Mumford-Shah functional [8]. In [11], Vese and Chan proposed a *piecewise smooth (PS)* model, which overcomes the limitation of their original work [2]. But these methods are computationally inefficient. The technique proposed by Tsai *et al.* [10] can address the segmentation of images with intensity inhomogeneity. However, the computation in their method is also expensive. As proposed in [10], one way to reduce the computational cost is to use a contour near the object boundaries as the initial contour. In their method, such initial contour is obtained by a preliminary segmentation using other active contour models, such as Chan and Vese's PC model. However, for images with intensity inhomogeneity, PC model can result in a contour that is still far

1-4244-1180-7/07/$25.00 ©2007 IEEE

away from the object boundary. In this situation, their two-stage approach still cannot significantly reduce the computational cost.

In fact, intensity inhomogeneity occurs in many real images of different modalities. In particular, it is often seen in medical images, such as X-ray radiography/tomography and magnetic resonance (MR) images, due to technical limitations or artifacts introduced by the object being imaged. For example, intensity inhomogeneity typically appears in MR images (see Fig. 4 for example). The inhomogeneity in MR images arises from non-uniform magnetic field produced by radio-frequency coils as well as from object susceptibility. The degree of this inhomogeneity is worse for higher field imaging (e.g., 7T MR) which is being increasingly used in research. Therefore, overcoming the difficulty of segmentation due to image inhomogeneity is a main motivation of this paper.

In this paper, we propose a novel active contour model that is able to segment images with intensity inhomogeneity. The basic idea is to introduce a kernel function to define a local binary fitting energy in a variational formulation, so that local intensity information can be embedded into a region-based active contour model. The local binary fitting energy functional is further incorporated into a variational level set formulation without reinitialization proposed by Li *et al.* [6]. Therefore, no reinitialization is necessary in the proposed method.

2. Background

2.1. Mumford-Shah functional for image segmentation

Let $\Omega \subset \Re^2$ be the image domain, and $I : \Omega \to \Re$ be a given image. In [8], Mumford and Shah formulated image segmentation as a problem of seeking an optimal contour C that divides the image domain into disjoint subregions, and an optimal function u that fits the original image I and that is smooth within each of the subregions. They proposed the following energy functional:

$$F^{MS}(u, C) = \int_{\Omega} (I-u)^2 dxdy + \nu \int_{\Omega \setminus C} |\nabla u|^2 dxdy + \nu |C| \tag{1}$$

where $|C|$ is the length of contour C. Thus, image segmentation can be performed by minimizing the above functional over all the contours and fitting function u. However, it is difficult to minimize the above functional (1), due to different nature of the two unknowns: a contour C and a function u, and the non-convexity of the functional as well. For practical applications, much works have been done to simplified or modified the above Mumford-Shah functional, including the two well known approaches that are reviewed below.

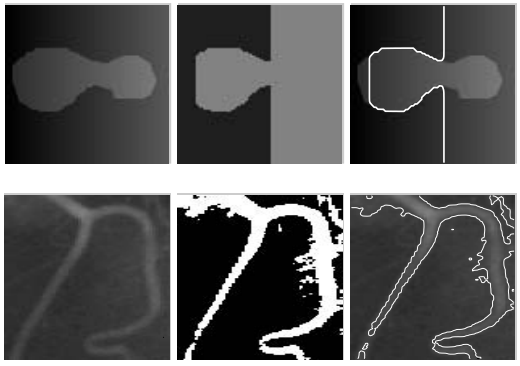

Figure 1. Error of thresholding and Chan-Vese model for images with intensity inhomogeneity. Column 1: Original images; Column 2: Thresholding results; Column 3: Results of PC model.

2.2. Piecewise constant model using active contours

Chan and Vese [2] proposed an active contour approach to the Mumford-Shah problem for a special case where the image u in the functional (1) is a piecewise constant function. For an image $I(x, y)$ on the image domain Ω, they proposed to minimize the following energy

$$\begin{aligned} E^{CV}(C, c_1, c_2) &= \lambda_1 \int_{in(C)} |I(\mathbf{x}) - c_1|^2 d\mathbf{x} \\ &+ \lambda_2 \int_{out(C)} |I(\mathbf{x}) - c_2|^2 d\mathbf{x} + \nu |C| \end{aligned} \tag{2}$$

where $in(C)$ and $out(C)$ represent the region inside and outside of the contour C, respectively, and c_1 and c_2 are two constants that approximate the image intensity in $in(C)$ and $out(C)$. We call the first two terms in (2) the *global binary fitting energy*. This energy can be represented by a level set formulation, and then energy minimization problem can be converted to solving a level set evolution equation [2].

In the above Chan-Vese model, the constants c_1 and c_2 are introduced to fit the image intensities in the regions $in(C)$ and $out(C)$, respectively. Obviously, such global fitting will not be accurate if the image intensities in either $in(C)$ or $out(C)$ are not homogeneous. This is the reason why Chan-Vese model [2] cannot handle intensity inhomogeneity. Similarly, Vese and Chan's piecewise constant model in a multiphase level set framework [11] still cannot address intensity inhomogeneity.

For example, the synthetic image and the real vessel image in Fig. 1 are typical examples of images with intensity inhomogeneity. In the vessel image, the intensity in the background decreases gradually from the top to the bottom. Moreover, part of the background (the upper left corner) has even higher intensities than part of the vessel (the

lower left branch). The second and the third columns of Fig. 1 show the segmentation results using thresholding and the PC model, respectively. It is clearly seen that part of the background is incorrectly identified as the foreground, while part of the foreground is labeled as the background.

2.3. Piecewise smooth model and its difficulties

The PS models proposed by Vese and Chan [11] and Tsai *et al.* [10] have overcome the difficulties of PC models in the presence of image inhomogeneity. Instead of approximating an image I by a piecewise constant function, the PS model approximates the image by two smooth functions $u^+(\mathbf{x})$ and $u^-(\mathbf{x})$ in the subregions $\Omega^+ = \{\mathbf{x} \in \Omega : \phi(\mathbf{x}) < 0\}$ and $\Omega^- = \{\mathbf{x} \in \Omega : \phi(\mathbf{x}) < 0\}$, respectively. By definition, the functions u^+ and u^- are defined on two exclusive subregions Ω^+ and Ω^-, respectively. However, the level set evolution equation derived to minimize the energy functional in the PS model is with respect to the level set function ϕ, which is defined on the full domain Ω. Therefore, there is an unavoidable step that extends u^+ and u^- to the full domain Ω. Moreover, the smoothness of the functions u^+ and u^- is enforced by the smoothing terms $\mu \int |\nabla u^+|^2 d\mathbf{x}$ and $\mu \int |\nabla u^-|^2 d\mathbf{x}$ in the energy functional in the PS model, which leads to two PDEs with the unknown functions u^+ and u^- that have to be solved at each iteration of the level set function ϕ.

In addition, it is necessary to periodically reinitialize the level set function ϕ to a signed distance function in practical application of the PS model. In summary, the need of solving PDEs for u^+ and u^-, the extension of u^+ and u^-, and the reinitialization makes the PS model computationally very expensive. Moreover, these procedures introduce quite a few parameters to the PS models, which increases the difficulty of selecting parameters in using the PS model, especially for inexperienced users.

3. Local binary fitting active contour model and its level set formulation

3.1. Active contours with local binary fitting energy

Consider a given vector valued image $I : \Omega \to \Re^d$, where $\Omega \subset \Re^n$ is the image domain, and $d \geq 1$ is the dimension of the vector $I(\mathbf{x})$. For gray level images, $d = 1$, for color images, $d = 3$. Let C be a contour in the image domain Ω. We define for each point $\mathbf{x} \in \Omega$ the following energy

$$\begin{aligned} & \mathcal{E}_{\mathbf{x}}^{LBF}(C, f_1(\mathbf{x}), f_2(\mathbf{x})) \\ = \; & \lambda_1 \int_{in(C)} K(\mathbf{x}-\mathbf{y}) |I(\mathbf{y}) - f_1(\mathbf{x})|^2 d\mathbf{y} \\ + \; & \lambda_2 \int_{out(C)} K(\mathbf{x}-\mathbf{y}) |I(\mathbf{y}) - f_2(\mathbf{x})|^2 d\mathbf{y} \end{aligned} \quad (3)$$

where λ_1 and λ_2 are positive constants, and K is a kernel function with a localization property that $K(\mathbf{u})$ decreases and approaches zero as $|\mathbf{u}|$ increases, and $f_1(\mathbf{x})$ and $f_2(\mathbf{x})$ are two numbers that fit image intensities near the point $\mathbf{x}$. We call the point $\mathbf{x}$ the *center point* of the above integral, and the above energy the *local binary fitting (LBF) energy* around the center point $\mathbf{x}$.

In this paper, we choose the kernel function $K(\mathbf{x})$ as a Gaussian kernel

$$K_\sigma(\mathbf{x}) = \frac{1}{(2\pi)^{n/2}\sigma^n} e^{-|\mathbf{x}|^2/2\sigma^2}, \quad (4)$$

with a scale parameter $\sigma > 0$. It should be emphasized that the numbers f_1 and f_2 that minimize the energy (3) vary with the center point $\mathbf{x}$. The introduction of the spatially varying fitting functions f_1 and f_2 makes our method essentially different from piecewise constant models.

In the proposed model, the fitting energy in (3) is local to the center point $\mathbf{x}$ in the sense that the values f_1 and f_2 only fit the image intensities near each $\mathbf{x}$. This is due to the kernel function K with the above localization property that $K(\mathbf{x}-\mathbf{y})$ takes larger values at the points $\mathbf{y}$ near the center point $\mathbf{x}$, and it decreases to 0 as $\mathbf{y}$ goes away from $\mathbf{x}$. Therefore, the image intensities at the points $\mathbf{y}$ near the point $\mathbf{x}$ have dominant influence on the values of f_1 and f_2 that minimize $\mathcal{E}_{\mathbf{x}}^{LBF}(C, f_1, f_2)$, whereas the image intensities at the points $\mathbf{y}$ far away from the center point $\mathbf{x}$ have almost no influence on the values of f_1 and f_2.

As mentioned above, the values f_1 and f_2 that minimize the LBF energy $\mathcal{E}_{\mathbf{x}}^{LBF}(C, f_1, f_2)$ are functions of the center point $\mathbf{x}$ due to the localization property of the kernel function $K(\mathbf{x}-\mathbf{y})$. Obviously, for each center point $\mathbf{x}$, the local fitting energy $\mathcal{E}_{\mathbf{x}}^{LBF}$ can be minimized when the contour C is exactly on the object boundary and the fitting values f_1 and f_2 are chosen optimally. However, the above energy $\mathcal{E}_{\mathbf{x}}^{LBF}$ is defined locally for a center point $\mathbf{x} \in \Omega$. To find the entire object boundary, we must minimize $\mathcal{E}_{\mathbf{x}}^{LBF}$ for all the center points $\mathbf{x}$ in the image domain Ω. This can be achieved by minimize the integral of $\mathcal{E}_{\mathbf{x}}^{LBF}$ over all the center points $\mathbf{x}$ in the image domain Ω. So, we define the following energy functional

$$\mathcal{E}(C, f_1, f_2) = \int_\Omega \mathcal{E}_{\mathbf{x}}^{LBF}(C, f_1(\mathbf{x}), f_2(\mathbf{x})) d\mathbf{x} \quad (5)$$

This energy can be converted to an equivalent level set formulation, from which an implicit active contour model will be obtained to automatically handle topological changes (see below).

3.2. Variational level set formulation of the model

In level set methods, a contour $C \subset \Omega$ is represented by the zero level set of a Lipschitz function $\phi : \Omega \to \Re$.

With the level set representation, the energy functional $\mathcal{E}_{\mathbf{x}}^{LBF}(C, f_1(\mathbf{x}), f_2(\mathbf{x}))$ in (3) can be rewritten as

$$\begin{aligned} & \mathcal{E}_{\mathbf{x}}^{LBF}(\phi, f_1(\mathbf{x}), f_2(\mathbf{x})) \\ = \; & \lambda_1 \int K_\sigma(\mathbf{x}-\mathbf{y})|I(\mathbf{y})-f_1(\mathbf{x})|^2 H(\phi(\mathbf{y}))d\mathbf{y} \\ + \; & \lambda_2 \int K_\sigma(\mathbf{x}-\mathbf{y})|I(\mathbf{y})-f_2(\mathbf{x})|^2 (1-H(\phi(\mathbf{y})))d\mathbf{y} \end{aligned} \tag{6}$$

where H is the Heaviside function. Thus, the fitting energy $\mathcal{E}$ in Eq. (5) can be written as

$$\begin{aligned} & \mathcal{E}^{LBF}(\phi, f_1, f_2) \\ = \; & \int_\Omega \mathcal{E}_{\mathbf{x}}^{LBF}(\phi, f_1(\mathbf{x}), f_2(\mathbf{x}))d\mathbf{x} \\ = \; & \lambda_1 \int [\int K_\sigma(\mathbf{x}-\mathbf{y})|I(\mathbf{y})-f_1(\mathbf{x})|^2 H(\phi(\mathbf{y}))d\mathbf{y}]d\mathbf{x} \\ + \; & \lambda_2 \int [\int K_\sigma(\mathbf{x}-\mathbf{y})|I(\mathbf{y})-f_2(\mathbf{x})|^2 \\ & \cdot(1-H(\phi(\mathbf{y})))d\mathbf{y}]d\mathbf{x} \end{aligned} \tag{7}$$

In order to ensure stable evolution of the level set function ϕ, we add the distance regularizing term in Li *et al.*'s variational level set formulation [6] to penalize the deviation of the level set function ϕ from a signed distance function. The deviation of the level set function ϕ from a signed distance function is characterized by the following integral

$$\mathcal{P}(\phi) = \int_\Omega \frac{1}{2}(|\nabla\phi(\mathbf{x})|-1)^2 d\mathbf{x} \tag{8}$$

To regularize the zero level contour of ϕ, we also need the length of the zero level curve (surface) of ϕ, which is given by

$$\mathcal{L}(\phi) = \int_\Omega \delta(\phi(\mathbf{x}))|\nabla\phi(\mathbf{x})|d\mathbf{x} \tag{9}$$

Now, we define the entire energy functional

$$\mathcal{F}(\phi, f_1, f_2) = \mathcal{E}^{LBF}(\phi, f_1, f_2) + \mu\mathcal{P}(\phi) + \nu\mathcal{L}(\phi) \tag{10}$$

where μ and ν are nonnegative constants.

In practice, the Heaviside function H in Eq. (6) is approximated by a smooth function H_ε defined by

$$H_\varepsilon(x) = \frac{1}{2}[1+\frac{2}{\pi}\arctan(\frac{x}{\varepsilon})] \tag{11}$$

The derivative of H_ε is the following smooth function

$$\delta_\varepsilon(x) = H'_\varepsilon(x) = \frac{1}{\pi}\frac{\varepsilon}{\varepsilon^2+x^2} \tag{12}$$

By replacing H and δ in (7) and (9) with H_ε and δ_ε, the energy functionals $\mathcal{E}^{LBF}$ and $\mathcal{L}$ are regularized as $\mathcal{E}_\varepsilon^{LBF}$ and $\mathcal{L}_\varepsilon$. As in [2, 11], we choose $\varepsilon = 1.0$ for good approximation of H and δ by H_ε and δ_ε. Thus, the energy functional $\mathcal{F}(\phi, f_1, f_2)$ in (10) is approximated by

$$\mathcal{F}_\varepsilon(\phi, f_1, f_2) = \mathcal{E}_\varepsilon^{LBF}(\phi, f_1, f_2) + \mu\mathcal{P}(\phi) + \nu\mathcal{L}_\varepsilon(\phi) \tag{13}$$

This is the energy functional we will minimize to find the object boundary.

3.3. Gradient descent flow

We use the standard gradient descent (or steepest descent) method to minimize the energy functional (13). The derivation of the gradient flow is similar to that of the PC and PS models in [2, 11]. The detailed procedure is given as the following.

For a fixed level set function ϕ, we minimize the functional $\mathcal{F}_\varepsilon(\phi, f_1, f_2)$ in (13) with respect to the functions $f_1(\mathbf{x})$ and $f_2(\mathbf{x})$. By calculus of variations, it can be shown that the functions $f_1(\mathbf{x})$ and $f_2(\mathbf{x})$ that minimize $\mathcal{F}_\varepsilon(\phi, f_1, f_2)$ for a fixed function ϕ are given by

$$f_1(\mathbf{x}) = \frac{K_\sigma(\mathbf{x}) * [H_\varepsilon(\phi(\mathbf{x}))I(\mathbf{x})]}{K_\sigma(\mathbf{x}) * H_\varepsilon(\phi(\mathbf{x}))} \tag{14}$$

and

$$f_2(\mathbf{x}) = \frac{K_\sigma(\mathbf{x}) * [(1-H_\varepsilon(\phi(\mathbf{x})))I(\mathbf{x})]}{K_\sigma(\mathbf{x}) * [1-H_\varepsilon(\phi(\mathbf{x}))]} \tag{15}$$

Note that the denominators in (14) and (15) are always positive, due to the fact that $H_\varepsilon(\phi) > 0$ and $1 - H_\varepsilon(\phi) > 0$ by the definition of H_ε in (11).

Keeping f_1 and f_2 fixed, and minimizing the energy functional $\mathcal{F}_\varepsilon(\phi, f_1, f_2)$ with respect to ϕ, we derive the gradient descent flow:

$$\begin{aligned} \frac{\partial\phi}{\partial t} = \; & -\delta_\varepsilon(\phi)(\lambda_1 e_1 - \lambda_2 e_2) + \nu\delta_\varepsilon(\phi)\mathrm{div}\left(\frac{\nabla\phi}{|\nabla\phi|}\right) \\ + \; & \mu\left(\nabla^2\phi - \mathrm{div}\left(\frac{\nabla\phi}{|\nabla\phi|}\right)\right) \end{aligned} \tag{16}$$

where δ_ε is the smooth Dirac function given by (12), and e_1 and e_2 are the functions as below

$$e_1(\mathbf{x}) = \int_\Omega K_\sigma(\mathbf{y}-\mathbf{x})|I(\mathbf{x})-f_1(\mathbf{y})|^2 d\mathbf{y} \tag{17}$$

and

$$e_2(\mathbf{x}) = \int_\Omega K_\sigma(\mathbf{y}-\mathbf{x})|I(\mathbf{x})-f_2(\mathbf{y})|^2 d\mathbf{y} \tag{18}$$

where f_1 and f_2 are given by (14) and (15), respectively. The above equation (16) is the proposed implicit active contour model in this paper. We call this model *LBF* active contour model to distinguish it from the PC and PS models.

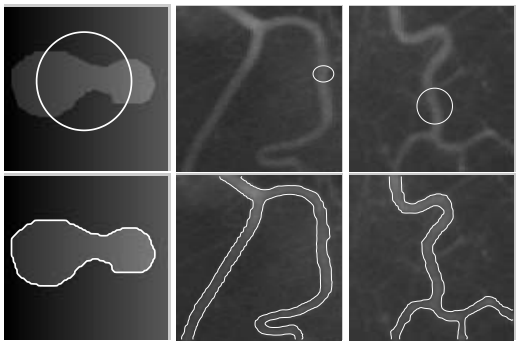

Figure 2. Application to two real blood vessel images and a synthetic image. Upper row: Original images and initial contours. Lower row: Final contours.

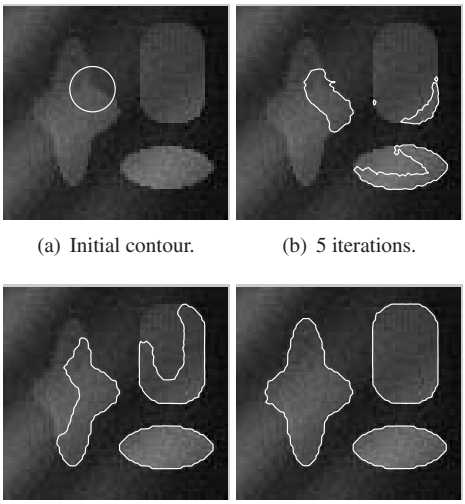

(a) Initial contour. (b) 5 iterations.

(c) 15 iterations. (d) 60 iterations.

Figure 3. Application to a noisy synthetic image.

3.4. Advantages of our model

In contrast to PS model [11], in our model, it is not necessary to regularize the fitting functions f_1 and f_2. In fact, it can be shown that the functions f_1 and f_2 minimizing the functional (13) is given by (14) and (15). They are are smooth functions due to the Gaussian convolutions in the derived formulas (14) and (15). Moreover, there is no need for extension of f_1 and f_2 in our model, since they are naturally defined on the full domain Ω.

Another advantage of our model is that no reinitialization is necessary in our method, due to the distance regularizing term (8). Moreover, our method with distance regularizing term allows for flexible initialization of level set function ϕ. In particular, we can simply initialize ϕ as a binary function, which takes a constant value c_0 in a region R_0 and $-c_0$ outside of R_0, where R_0 can be an arbitrarily given subset in the image domain Ω.

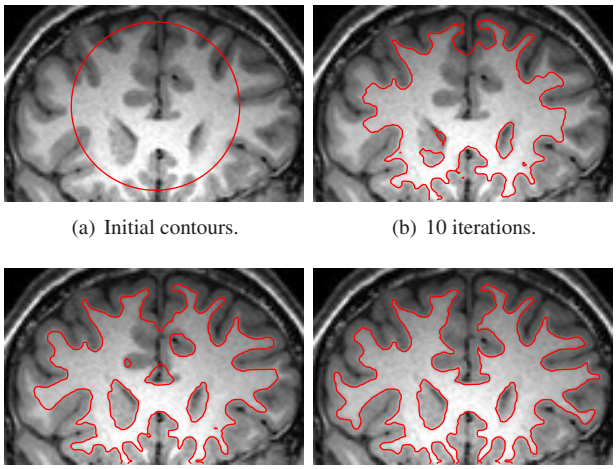

(a) Initial contours. (b) 10 iterations.

(c) 50 iterations. (d) 200 iterations.

Figure 4. Application to white matter segmentation for MR image.

4. Implementation and results

To compute the functions f_1 and f_2 given by Eq. (14) and (15), we can use the efficient FFT to compute the convolution operations. The term $\lambda_1 e_1 - \lambda_2 e_2$ in (16) can be written as a linear combination of three convolutions. All the partial derivatives $\frac{\partial \phi}{\partial x}$ and $\frac{\partial \phi}{\partial y}$ in (16) are approximated using the simple finite difference scheme in [6]. Our method has been applied to synthetic and real images of different modalities. We use the same parameters of $\nu = 0.001 \times 255^2$, time step $\tau = 0.1$, $\mu = 1.0$, and $\sigma = 3.0$, $\lambda_1 = \lambda_2 = 1.0$ for all the images in this paper, except the one in Fig. 4, for which we set $\nu = 0.003 \times 255^2$, $\lambda_1 = 1.0$ and $\lambda_2 = 2.0$.

4.1. Results of our method

We first show the results of our method for a synthetic image and two blood vessel images shown in Fig. 2. The initial contours and the final contours are shown in the upper row and the lower row, respectively. In these images, both the background and the foreground exhibit obvious intensity inhomogeneity. Note that the synthetic image in the first column and the vessel image in the second column are the same images in Fig. 1, which has shown that the PC model fails to segment the object correctly. In the vessel images, some parts of the vessel boundaries in these two images are quite weak. As can be seen from the lower row of Fig. 2, our model achieves satisfactory segmentation results for these three images.

Fig. 3 shows the result of our method for a noisy synthetic image with three objects, and with serious intensity inhomogeneity. For this image, the initial contour was placed across one object and the background as in Fig. 3(a). It is worth pointing out that new contours can emerge during

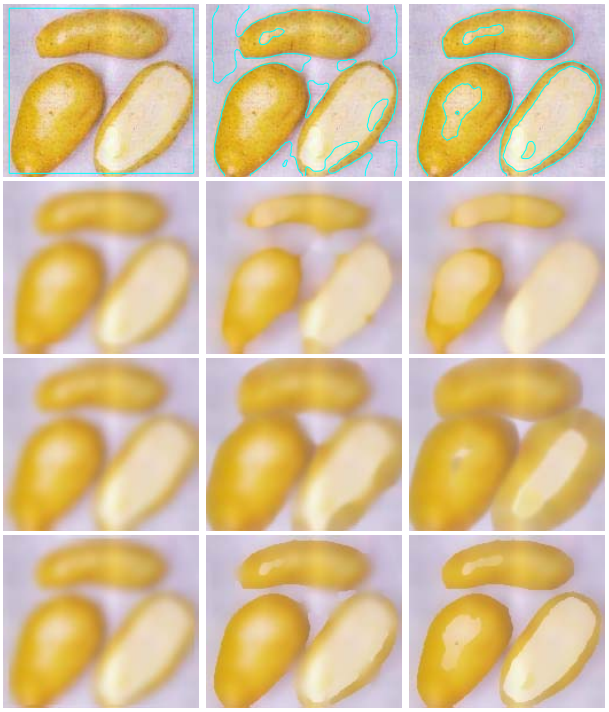

Figure 5. Results for a real color image of potatoes. Row 1: Contours on the original image; Row 2: Image f_1; Row 3: Image f_2; Row 4: Fitting image $H_\varepsilon(\phi)f_1 + (1 - H_\varepsilon(\phi))f_2$.

the evolution, which can be seen from the curve evolution process as depicted in Fig. 3(b), 3(c), and 3(d) for iterations 5, 15, and 60, respectively. The final contours recover all the three object boundaries very well, as shown in Fig. 3(d). It is worth pointing out that our method is also able to segment images consisting of multiple homogeneous regions with distinct means, which is a special case of intensity inhomogeneity.

As mentioned in the introduction, intensity inhomogeneity is also typical in MR images. Fig. 4 shows the result for an MR image of human brain, which shows obvious intensity inhomogeneity. In fact, the intensity of white matter in the upper part is even lower than that of the gray matter in the lower part. The curve evolution is depicted in Fig. 4, which shows successful segmentation of the white matter in this image. Note that, we used a larger value of ν for this image than those for the other images to prevent the emergence of new contours at the boundaries of unwanted structures like the skull.

The proposed method has also been applied to 3D magnetic resonance angiography (MRA) images for segmentation of cerebral vasculature. For example, Fig. 6(a) shows the maximum intensity projection (MIP) of a 3D MRA image. The image size is $300 \times 300 \times 60$ voxels with spacing of $0.195mm \times 0.195mm \times 0.5mm$. For this 3D image, we use the parameters $\lambda = 0.01 \times 255^2$, $\tau = 0.1$, $\mu = 1.0$,

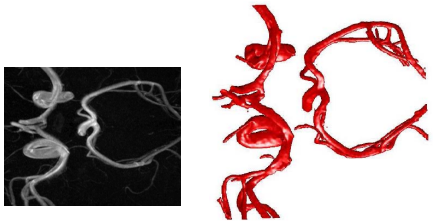

(a) MIP. (b) Final surface of our method.

Figure 6. Application to 3D MRA image segmentation.

and $\sigma = 2.0$. The final surface obtained by our method is shown in Fig. 6(b).

Fig. 5 shows the results for a real color image of potatoes, which demonstrates the joint segmentation and denoising by using the LBF model. The first row plots the active contours on the original images from its initial to converged state. The second and third rows show the corresponding fitting images f_1 and f_2, computed by (14) and (15) respectively.

As a natural application of our LBF model, the final fitting functions f_1 and f_2 and the level set function ϕ can be used for image denoising. We define the following fitting image

$$f = H_\varepsilon(\phi)f_1 + (1 - H_\varepsilon(\phi))f_2 \tag{19}$$

The above computed image f can be used to approximate the original image while reducing the noise. The fourth row in Fig. 5 shows the evolution of the fitting image f computed by (19). When the level set function ϕ converges, the fitting image f (shown in the right most images in the fourth row) fits the original image very well with noise significantly reduced. Moreover, the boundaries of meaningful regions are enhanced.

4.2. Comparison with piecewise smooth model

The results of the PC model (shown in Fig. 1) and the results of our method (Fig. 2) have demonstrated the obvious advantage of our method. Now, we focus on the comparison of our model with the PS model. The PS model is computationally very expensive due to its complex procedure described in Section 2.3. We have implemented Vese and Chan's PS model in [11]. Note that, in our implementation of the PS model in [11], reinitialization is necessary for many typical images, including those in this paper. By contrast, due to the distance regularizing term (8) in our LBF energy functional (13), no reinitialization is necessary in our method.

Fig. 7 shows the results of our model (the upper row) and the PS model (the lower row) using the same initial contours. The CPU times for these images are listed in Table 1, which were recorded from our experiments with Mat-

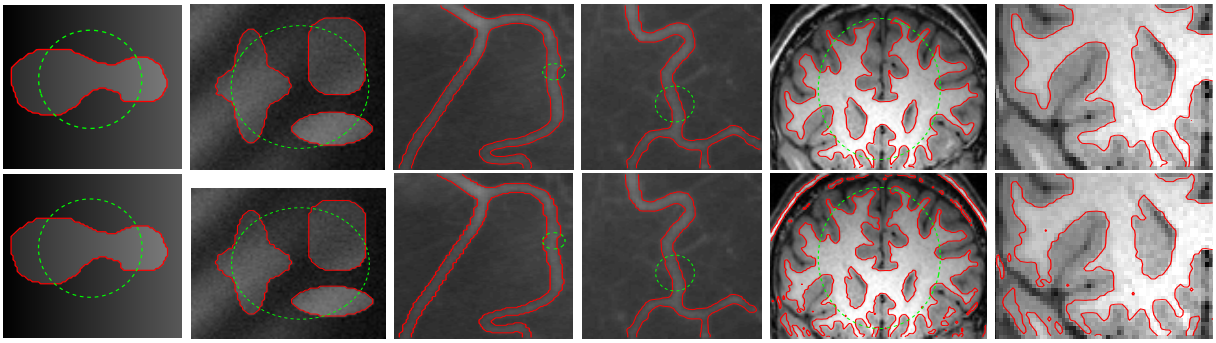

Figure 7. Comparison of our method with PS model. The initial contours and the final contours are plotted as the dashed green contours and solid red contours, respectively. Upper row: The results of our method; Lower row: The results of PS model.

	Img1	Img2	Img3	Img4	Img5
LBF	1.78	2.42	16.04	11.85	9.81
PS	39.92	101.89	398.45	203.03	120.52

Table 1. CPU time (in second) for LBF model and PS model for the images in Fig. 7 in the same order.

lab code run on a Dell Dimension 4600 PC, with Pentium 4 processor, 2.80 GHz, 1GB RAM, with Matlab 6.5 on Windows XP. It is obvious that our model is significantly faster than the PS model. In the experiments with the images in Fig. 7, our model is about 15 to 40 times faster than the PS model. This demonstrates the significant advantage of our model in terms of computational efficiency.

Our model is also superior in terms of accuracy, due to its capability of utilizing local image information. This is obvious for the MR image in the fifth column in Fig. 7. Our method extracts the white matter boundary accurately, while the contour of the PS model skips white matter boundary and is finally attracted to the outer boundary of gray matter. In addition, some unwanted contours were generated in the result of PS model. The right most column in Fig. 7 is an enlarged view of the lower left portion of the figures in the fifth column, which clearly shows the superior result of our model to that of the PS model. For the first three images in Fig. 7, the results both models appear to be similar, but the final contours of the PS model are somewhat noisy.

5. Conclusions

In this paper, we propose a novel region-based active contour model for image segmentation in a variational level set framework. The proposed method efficiently utilizes local image information, and therefore is able to segment images with intensity inhomogeneity. Experimental results also demonstrate desirable performance of our method for images with weak object boundaries and vessel-like structures. Comparisons with piecewise smooth model show the advantages of our model in terms of efficiency and accuracy. In addition, the proposed method has promising application to image denoising.

References

[1] V. Caselles, R. Kimmel, and G. Sapiro. Geodesic active contours. *Int'l J. Comp. Vis.*, 22:61–79, 1997.

[2] T. Chan and L. Vese. Active contours without edges. *IEEE Trans. Imag. Proc.*, 10:266–277, 2001.

[3] L. Cohen and I. Cohen. Finite-element methods for active contour models and balloons for 2-D and 3-D images. *IEEE Trans. Patt. Anal. Mach. Intell.*, 15:1131–1147, 1993.

[4] M. Kass, A. Witkin, and D. Terzopoulos. Snakes: active contour models. *Int'l J. Comp. Vis.*, 1:321–331, 1987.

[5] C. Li, J. Liu, and M. D. Fox. Segmentation of external force field for automatic initialization and splitting of snakes. *Pattern Recognition*, 38(11):1947–1960, 2005.

[6] C. Li, C. Xu, C. Gui, and M. D. Fox. Level set evolution without re-initialization: A new variational formulation. In *IEEE Conference on Computer Vision and Pattern Recognotion (CVPR).*, volume 1, pages 430–436, 2005.

[7] R. Malladi, J. A. Sethian, and B. C. Vemuri. Shape modeling with front propagation: a level set approach. *IEEE Trans. Patt. Anal. Mach. Intell.*, 17:158–175, 1995.

[8] D. Mumford and J. Shah. Optimal approximations by piecewise smooth functions and associated variational problems. *Commun. Pure Appl. Math.*, 42:577–685, 1989.

[9] N. Paragios and R. Deriche. Geodesic active regions and level set methods for supervised texture segmentation. *Int'l J. Comp. Vis.*, 46:223–247, 2002.

[10] A. Tsai, A. Yezzi, and A. S. Willsky. Curve evolution implementation of the mumford-shah functional for image segmentation, denoising, interpolation, and magnification. *IEEE Trans. Imag. Proc.*, 10:1169–1186, 2001.

[11] L. Vese and T. Chan. A multiphase level set framework for image segmentation using the mumford and shah model. *Int'l J. Comp. Vis.*, 50:271–293, 2002.

[12] C. Xu and J. Prince. Snakes, shapes, and gradient vector flow. *IEEE Trans. Imag. Proc.*, 7:359–369, 1998.